PAPER

Rare earth (RE – Ce, Gd) modified Nd$_{1-x}$RE$_x$FeAsO$_{0.7}$F$_{0.3}$ superconductor with enhanced magneto-transport properties

P. M. Aswathy,[a] J. B. Anooja,[a] Neson Varghese,[a] C. K. Chandrakanth,[a] N. Devendra Kumar,[b] A. Sundaresan[c] and U. Syamaprasad*[a]

The influence of rare earth (RE – Ce, Gd) doping at the Nd site in the NdFeAsO$_{0.7}$F$_{0.3}$ superconductor wherein Ce and Gd have ionic radii in the order Ce > Nd > Gd is investigated. The structural and superconductivity characterization of the pure and doped samples show that Ce doping enhances the T_C of Nd$_{1-x}$RE$_x$FeAsO$_{0.7}$F$_{0.3}$ to a maximum of 53.6 K at $x = 0.1$ while Gd doping attains a T_C of 55.1 K at $x = 0.15$. Interestingly, both Ce and Gd doping create neither secondary phases nor precipitates within the detection limit of XRD. However, the lattice defects due to Ce and Gd doping modifies NdFeAsO$_{0.7}$F$_{0.3}$ and assists in pinning the flux lines on these defects thereby exhibiting an enhanced $J_C(H)$ performance especially at high fields. It is also observed that the relatively small ionic size of Gd is more effective in T_C enhancement, while the lattice defects due to larger ionic size of Ce favor the remarkable enhancement of $J_C(H)$.

Introduction

With the discovery of superconductivity in LaFeAsO$_{1-x}$F$_x$ at 26 K by Hosono's group, the area of superconductivity witnessed research into a series of other iron based compounds having different crystal structures and interesting superconducting as well as magnetic properties.[1–3] Presently, the focus is to enhance the transport current and to utilize the very high upper critical field in iron pnictides for practical applications.[4] Apart from the explorations on application point of view, basic research through chemical doping is also being carried out at various sites of REFeAsO iron pnictides.[5–8] The REFeAsO system (abbreviated as RE1111 – RE refers to rare earth) shows a tetragonal to orthorhombic structural phase transition in between 100–200 K accompanied by a spin-density-wave (SDW) type antiferromagnetic long-range ordering.[9] The suppression of these structural and magnetic phase transitions is a major hurdle to induce superconductivity in this class of iron pnictides. Doping in the charge reservoir block (RE$_2$O$_2$ layer) and application of external pressure are effective methods to cause structural modification or balance in charge carrier concentration, which in turn induces superconductivity into the system.[2,3] Generally, fluorine substitution at oxygen site suppresses the

SDW instability and retains the tetragonal structure below 100 K leading to superconductivity. Further, it also causes lattice contraction especially along the c axis. Application of external pressure induces superconductivity as an aftereffect of the increase in charge transfer between the charge reservoir layer (RE$_2$(O/F)$_2$) and conducting FeAs layer due to the mechanically forced lattice contraction. In short, the RE1111 compounds show signs of superconductivity or enhancement in critical temperature (T_C) only if lattice contraction is induced by internal chemical pressure or external pressure.[10–12]

In RE1111, instead of fluorine doping at oxygen site, the substitution of RE with either an isovalent or aliovalent ion in the former enhances internal chemical pressure for a dopant of smaller ionic radius and the latter produces superconductivity by the variation in charge carrier concentration.[10,13] For iso-valent doping, fixed fluorine to oxygen ratio or oxygen vacancy is essential. Here, we can expect a T_C enhancement in rare-earth doped sample when compared to the solo fluorine doped RE1111 compound.[14] In aliovalent doping, fluorine doping is not mandatory and the solo substitution of a bivalent or tetra-valent ion at RE site in REFeAsO can give rise to superconductivity despite having a low T_C.[13] Cobalt or nickel doping at iron site and phosphorous doping at arsenic site have also been carried out to establish the relationship between the magnetic moments of Fe/Ln and superconductivity.[7,8,15]

The NdFeAsO$_{1-x}$F$_x$ (Nd1111) system, which is renowned for its very high upper critical field and almost constant critical current density at high fields, was initially reported to be superconducting under high pressure synthesis conditions.[16,17] Later, electron and hole-doped samples of Nd1111 processed at

^{a}*National Institute for Interdisciplinary Science and Technology (CSIR), Trivandrum 695019, India. E-mail: syamcsir@gmail.com; Fax: +91-471-2491712; Tel: +91-471-2515373*

^{b}*Department of Engineering, University of Cambridge, Cambridge CB2 1PZ, UK*

^{c}*Chemistry and Physics of Materials Unit, Jawaharlal Nehru Centre for Advanced Scientific Research, Bangalore 560064, India*

ambient pressures were also reported.[13,18] A lot of investigations were carried out to demonstrate the symmetry of electron and hole doping in iron pnictides. Often chemical doping is done with an aim to enhance the existing status of superconducting properties. For this, the dopants are chosen based on certain pre-requisites such as ionic-size-match and valency; not to mention the existence of sporadic reports contradictory to this requirement. In the present study, we have chosen two rare earth metals, Ce and Gd, for partial substitution of Nd in $NdFeAsO_{0.7}F_{0.3}$. Cerium is a magnetic rare earth with 4f electrons and variable valency (3 and 4). It is already known that cerium changes its valency upon cooling to very low temperatures and the oxidation state in the presence of other ions also varies. So the involvement of the valence electrons and their contribution to the total density of states in the Ce doped system remains intricate. Since the ionic size of Ce is larger than Nd, Ce substitution in Nd1111 is not expected to bring in a lattice contraction. However, the addition of Ce ions to the deliberate vacancies created at Nd site will definitely modulate the superconductivity observed in Nd1111 system. The dopant, Gd, is an isovalent ion for Nd and the ionic size of Gd is smaller than that of Nd. Thus, when compared to Nd, Ce is a larger ion with variable valency and Gd is a smaller isovalent ion. In this study, we present a detailed investigation of the effects of Ce and Gd doping at Nd site on the structural and superconducting properties of $NdFeAsO_{0.7}F_{0.3}$ superconductor.

Experimental

Polycrystalline samples of $Nd_{1-x}Ce_xFeAsO_{0.7}F_{0.3}$ ($x = 0, 0.1, 0.2$ and 0.3), named as NdCe0, NdCe1, NdCe2 and NdCe3, and $Nd_{1-x}Gd_xFeAsO_{0.7}F_{0.3}$ ($x = 0.1, 0.15$ and 0.2) named as NdGd1, NdGd15 and NdGd2 were synthesized using the solid state method based on the pre-processing technique reported elsewhere.[19] Stoichiometrically weighed powders of Nd, Ce, Gd, Fe, As, Fe_2O_3 and FeF_2 were mixed and ground using an agate mortar and pestle. All the samples were weighed, mixed and ground inside a glove box under high purity argon atmosphere.

The samples were compacted into rectangular pellets by applying pressure of 500 MPa using a hydraulic press. These pellets were then sealed in evacuated quartz tubes and heat treated in a muffle furnace under identical conditions. The samples followed a heat treatment procedure of 360 °C/5 h + 850 °C/30 h + 1000 °C/20 h with intermediate grinding and re-pelletizing. The clean, dense, rectangular pellets thus obtained were then subjected to structural and super-conducting analysis.

The phase identification of the samples was performed using powder X-ray diffractometer (PANalytical X' Pert Pro) with CuKα radiation employing a high-speed detector and a monochromator at the diffracted beam side. Microstructural examination was done on a scanning electron microscope (JEOL-JSM-5600LV). Superconducting transport measurements such as resistivity *versus* temperature (ρ–T) and current *versus* voltage (I–V) were carried out using a closed-cycle cryocooler integrated-cryostat (Janis Research Co., SHI SRDK-408 SW) by DC four-probe technique. The temperature dependence of ac susceptibility (χ–T) was measured using a closed-cycle ac susceptometer (ARS-CS202S-DMX-19 SCC and SR850). The temperature of the sample was precisely monitored using Lakeshore temperature controllers. DC magnetic measurements were carried out on parallelepiped samples with magnetic fields up to 6 T using a physical property measurement system (PPMS, Quantum Design). The field dependent resistivity measurements (0–9 T), Hall Effect and heat capacity measurements were also done using an in-house PPMS (Quantum Design).

Results and discussions

Fig. 1 shows the X-ray diffraction (XRD) patterns of the fine-powdered samples of (a) $NdFeAsO_{0.7}F_{0.3}$ (Nd3) and Ce doped $NdFeAsO_{0.7}F_{0.3}$ (NdCe1, NdCe2 and NdCe3) and (b) the Gd doped samples (NdGd1, NdGd15 and NdGd2). The phase identification of all these samples confirmed that the major phase is NdFeAsO which resembles the ZrCuSiAs type structure of $P4/nmm$ space group. Small amounts of impurity phases such
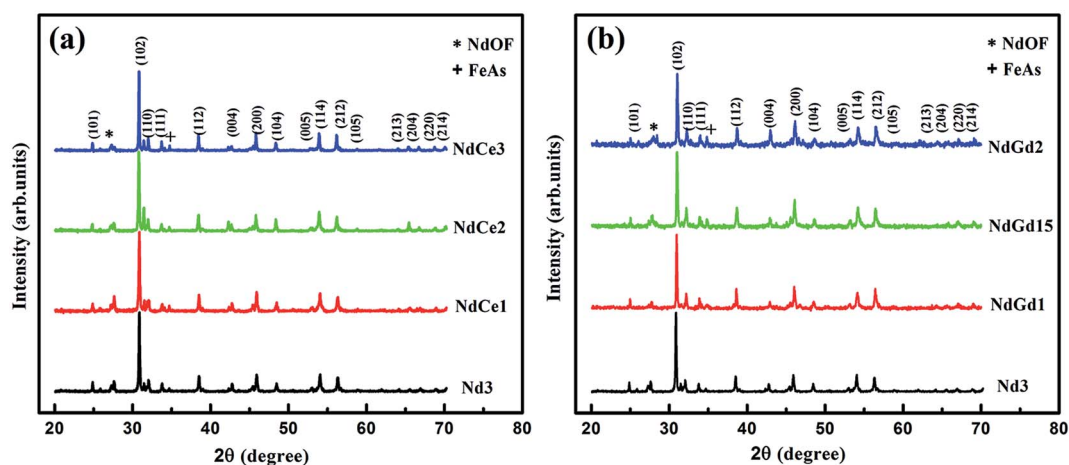

Fig. 1 XRD patterns of (a) pure (Nd3) and Ce doped Nd1111 samples and (b) pure (Nd3) and Gd doped Nd1111 samples.
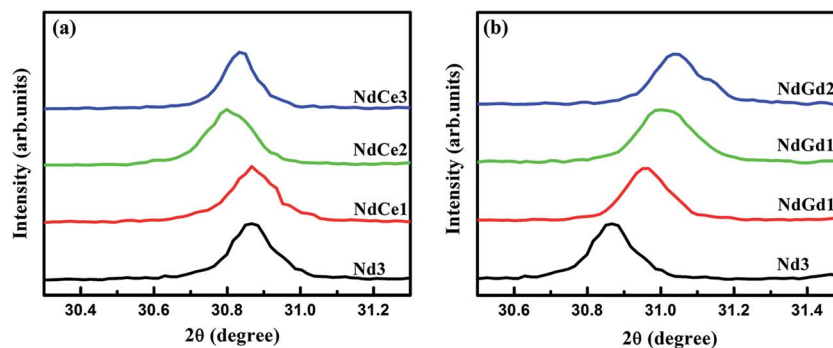
Fig. 2 Enlarged view of the main peak (102) in (a) Ce doped Nd1111 samples and (c) that of the Gd doped samples.

as NdOF and FeAs are also present in all the samples. However, phases of Ce and Gd or their derivatives have not been detected in any of the Ce and Gd doped Nd1111 samples. Moreover, the superconducting volume fraction is found to be more than 90% for all the samples. Fig. 2a and b show the enlarged view of XRD patterns around the main peak (102) for Ce and Gd doped samples keeping Nd3 as a reference pattern. It is observed that the main peak of Ce doped samples shift towards the left with respect to that of Nd3 while in Gd doped samples the peak shifts towards the right. However, in Ce and Gd doped samples, the shift of the peaks is almost saturated for NdCe3 and NdGd2 samples, respectively. In order to understand the effect of Ce and Gd substitution on the crystal lattice of Nd1111 system, the lattice parameters of all the samples were calculated using the Rietveld refined XRD data. The variation in lattice parameters with respect to the varying Ce and Gd content is graphically represented in Fig. 3a and b, respectively. The lattice parameters a and c of the Ce doped samples are found to increase with an increase in Ce content and the values remain almost constant for $x = 0.2$ and 0.3. For Gd doped samples, the lattice parameters were found to decrease with Gd doping with no significant change above $x = 0.15$. On comparing the ionic radii of Ce^{3+} (1.01 Å) and Gd^{3+} (0.935 Å) with that of Nd^{3+} (0.983 Å), the influence of lanthanide contraction is expected to occur only for Gd doping since it is relatively smaller in ionic radius as compared to Nd. The observed lattice parameter variation confirms the fact that the crystal lattice of Gd doped Nd1111

samples experience an internal chemical pressure due to doping of smaller ions at Nd site and undergo lattice compression. Whereas in Ce doped Nd1111 samples increase in lattice parameter occurs due to the substitution of relatively larger ions at Nd site.

Fig. 4 shows the SEM images of freshly fractured surfaces of pure (Nd3), Ce doped (NdCe1 and NdCe3) and Gd doped (NdGd15 and NdGd2) samples. The morphology of samples varies from layered flaky grains with well-defined edges similar to that observed in cuprate superconductors[20] to fused layered structures while using Ce and Gd as dopants, respectively. Ce and Gd doping causes minor but notable changes in the microstructure of Nd1111. In the Ce doped sample NdCe1, it is seen that the flaky nature of the grains is sustained with enhanced grain connectivity, well-defined edges and density in general. As the concentration of Ce doping is increased from NdCe1 to NdCe3, the porosity of the sample increases and the microstructure appears as conglomerated grains. The microstructure of Gd doped samples show densely packed grains fused together. The surface morphology remains unaffected while varying Gd concentration from NdGd15 to NdGd2. The layered nature of pure Nd11111 system changes into a fused surface morphology when Gd is used as dopant.

Fig. 5 shows the temperature dependent resistivity of pure (Nd3), Ce doped (NdCe1, NdCe2 and NdCe3) and Gd doped (NdGd1, NdGd15 and NdGd2) samples and the inset shows an enlarged view around the transition. The pure sample,
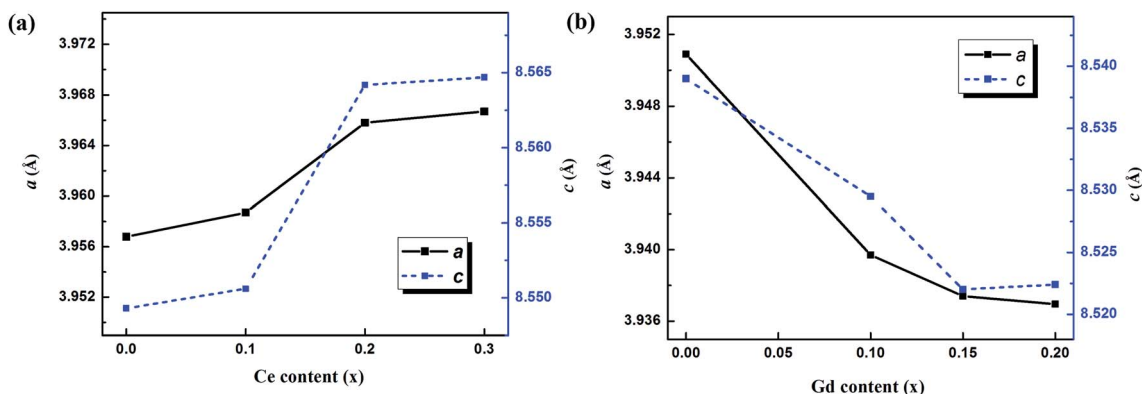

Fig. 3 Lattice parameter variation in (a) Ce doped Nd1111 samples and (b) Gd doped Nd1111 samples.
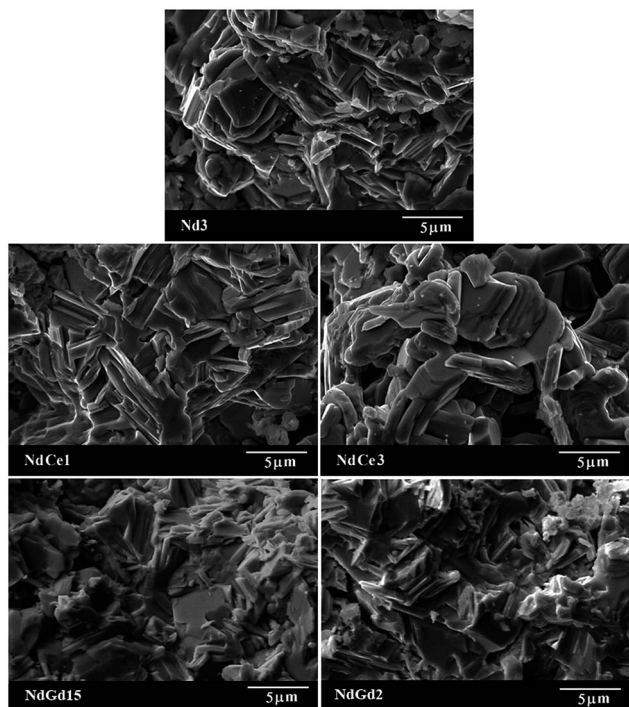
Paper

RSC Advances

Fig. 4 SEM images of freshly fractured surfaces of pure (Nd3), Ce doped Nd3 (NdCe1 and NdCe3) and Gd doped (NdGd15 and NdGd2) samples.
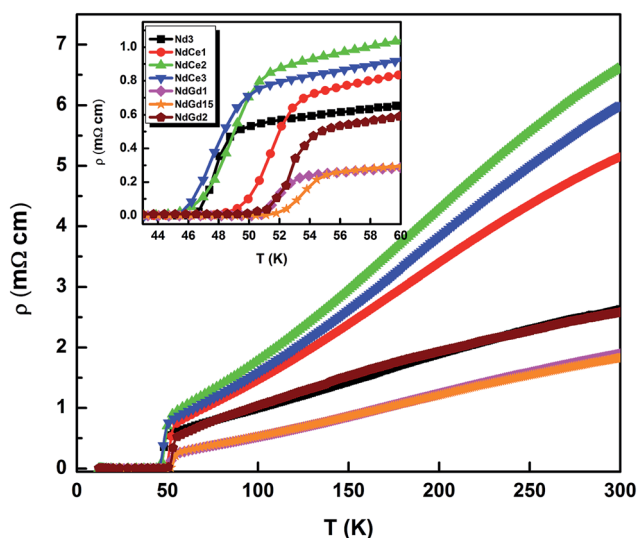

Fig. 5 Temperature dependent resistivity plots of pure (Nd3), Ce doped (NdCe1, NdCe2 and NdCe3) and Gd doped (NdGd1, NdGd15 and NdGd2) samples. Inset shows an enlarged view around the transition.

$NdFeAsO_{0.7}F_{0.3}$ shows metallic behavior up to the superconducting transition with a T_C around 48.8 K. Several attempts were made to increase the T_C of Nd1111 system following its first report on high pressure synthesis with a T_C of 51.9 K. $CeFeAsO_{1-x}F_x$ and $GdFeAsO_{1-x}F_x$ synthesized at ambient pressures exhibit a T_C of 41 K and 40.1 K, respectively and the mixed

Table 1 Superconducting parameters of pure, Ce and Gd doped Nd1111 samples

Sample name	T_C (K)		$\rho_{300\,K}$ (mΩ cm)	RRR
	ρ–T	χ–T		
Nd3	48.8	48.2	3.5	2.6
NdCe1	53.6	53.4	5.1	6.1
NdCe2	51.4	51.5	6.6	6.4
NdCe3	50.6	50.3	5.9	6.5
NdGd1	53.3	52.9	2.8	1.9
NdGd15	55.1	55	3.3	1.8
NdGd2	54.8	54.5	4.3	2.6

rare earth system $Ce_{1-x}Gd_xFeAsO_{0.84}F_{0.16}$ shows a maximum T_C of 47.5 K for $x = 0.4$.[9,21,22] It is fascinating to observe that both Ce and Gd doping in $NdFeAsO_{0.7}F_{0.3}$ enhanced the T_C of the system and the T_C values for all the samples are included in Table 1. All the samples remain metallic from room temperature up to their respective transition temperatures. The maximum T_C values attained due to Ce and Gd doping are 53.6 K ($x = 0.1$) and 55.1 K ($x = 0.15$), respectively. The normal state resistivity at room temperature (ρ_{300}) and residual resistivity ratio (RRR = ρ_{300}/ρ_{60}) are given in Table 1. Both ρ_{300} and RRR values are found to be higher for Ce doped samples compared to Nd3 whereas the values are comparable to that of Nd3 for Gd doped samples. Generally, lanthanides such as La, Nd, Sm and Gd exist as trivalent ions, but Ce changes its valency or oxidation state between 3 or 4, according to the compound in which it exists.[23] Since the 4f electrons in Ce are not fully localized, the charge density in the conducting block of Ce doped Nd1111 is unpredictable. However, in the present case, the increase in T_C of the samples with Ce doping confirms the enhancement in charge transfer between the charge reservoir and conducting layers favoring T_C enhancement. It is believed that elemental Ce doped in Nd1111 has a valency of 3 since modern purification methods yield trivalent Ce. However, at low temperatures a larger ion doping is not expected to cause T_C enhancement, but a change in valency can modulate the charge carrier density. Hence, it is presumed that the mixed valency nature exhibited by Ce at high pressures/low temperatures or change in local chemistry has helped in achieving an optimum charge density upon reaching the doping level of $x = 0.1$.[24] But the lattice mismatch caused by Ce substitution is found to increase the normal state resistivity and the RRR values are found to be relatively high. For Gd doping, lattice parameter reduction due to smaller isovalent ion substitution facilitates effective charge transfer. Thus, substitution of both smaller and larger ion at Nd site shows that lattice contraction due to smaller isovalent ions favors T_C enhancement in Gd doped system while in Ce doped system the condition is similar to the doping of aliovalent larger ions.

Fig. 6 shows the temperature dependent ac susceptibility plots of pure (Nd3), Ce doped (NdCe1, NdCe2 and NdCe3) and Gd doped (NdGd1, NdGd15 and NdGd2) samples measured at 0.49 mT ac field and 208 Hz signal frequency. The T_C values obtained through ac susceptibility measurement are in good
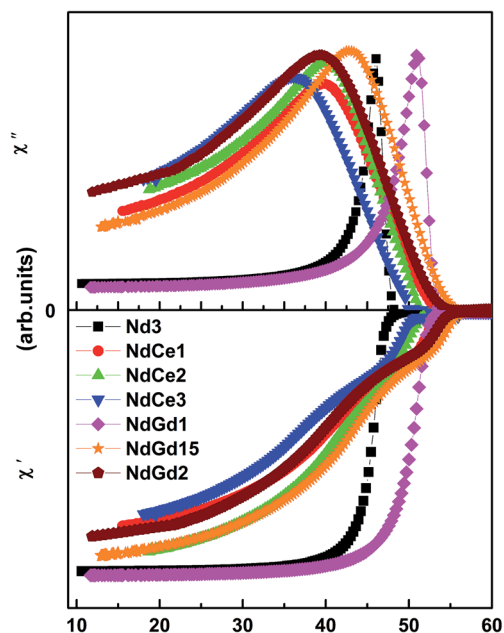
Fig. 6 Temperature dependent ac susceptibility plots of pure (Nd3), Ce doped (NdCe1, NdCe2 and NdCe3) and Gd doped (NdGd1, NdGd15 and NdGd2) samples.

Fig. 7 C_P/T versus T plots of pure (Nd3), Ce doped (NdCe1) and Gd doped (NdGd15) samples.

agreement with the resistivity data (Table 1). The ac susceptibility plot represents both the real (χ') and imaginary (χ'') parts with respect to temperature. The real part χ' evolves as a step-like diamagnetic transition on reaching a temperature corresponding to the T_C of the respective sample *i.e.* transition from near-perfect screening to complete penetration of external ac magnetic field into the sample; while χ'' forms a peak corresponding to this transition temperature and gives a measure of the dissipation in the sample.[25] In some cases, instead of single step sharp transition the real part exhibits a double-step or hump like behavior at a lower temperature. The two steps are attributed to the contributions from two types of current flowing in the sample: the intra-grain and inter-grain currents. The step near T_C represents intra-grain current and the step at a lower temperature represents inter-grain current. Often superconductors having electromagnetic granularity and mixed phases exhibit such double step transitions.[26,27] It is observed that almost all of the doped samples in the present study show double step transitions in χ' and a peak corresponding to the lower step in χ''. The inherent electromagnetic granularity of iron pnictides and the presence of similar phases at lower doping levels including the impurity phases are the reasons for this double stepping nature.

Apart from ρ–T and χ–T measurements, the samples were also subjected to calorimetric measurements so as to confirm the bulk superconductivity existing in the samples. At lower temperatures the average thermal energy available to each particle degree of freedom is smaller, and thermal energy storage becomes limited. Hence, as the temperature falls towards absolute zero, so does the heat capacity of a material. The specific heat capacity, *i.e.* heat capacity per unit mass, is an intensive bulk property that analyses the low energy electronic
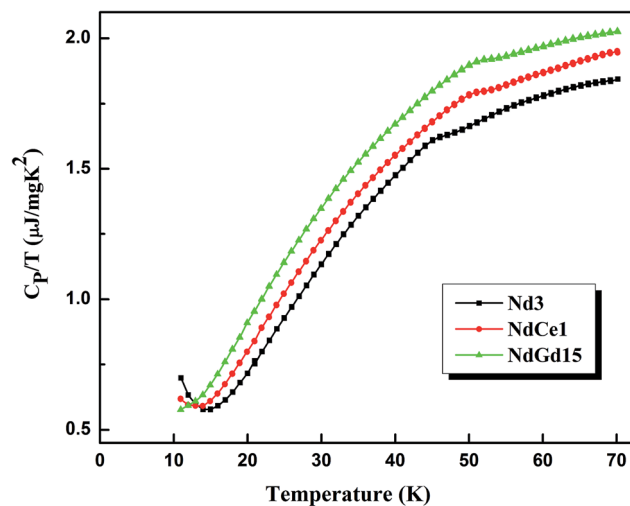
excitations at the Fermi level thereby enabling it to provide information on the density of states, the nature of the superconducting gap or unconventional gap states. Specific heat capacity of a material has temperature dependent contributions both from electrons and phonons. Thus, the temperature dependent behavior of specific heat capacity gives an idea on the phase transitions, thermal fluctuations and anisotropy within the sample. In the present case, Fig. 7 shows the temperature dependent heat capacity (C_P/T versus T) plots of Nd3, NdCe1 and NdGd15 at 0 T. It is observed that specific heat decreases linearly for all the samples down to their respective superconducting transition temperatures. Small step-like humps are observed near T_C and thereafter the specific heat values decrease rapidly. The onset T_C *i.e.* the temperatures at which the slight increase in C_P occur are found to be around 47, 53, and 54 K for Nd3, NdCe1 and NdGd15, respectively. These transitions are not as distinct as in the case of ρ–T and χ–T plots. Moreover, the humps in C_P are found to be smaller as compared to that observed in the Nd1111 single crystal reported elsewhere.[28] The doped samples display a relatively higher specific heat value and their ΔC_P near T_C is also relatively larger as compared to the pure sample, Nd3. At very low temperatures *i.e.* around 10 K, an upturn is observed in the specific heat which is an indicator of the Schottky anomaly due to the paramagnetic ions present in the sample.[29]

In order to understand the role of charge carrier density in the enhancement of T_C in the doped samples NdCe1 and NdGd15 as compared to Nd3, Hall Effect measurements were carried out on rectangular pieces of the samples. The voltage leads were connected perpendicular to the current leads, across an approximate equipotential line in the center keeping the applied field perpendicular to the plane of the sample. The Hall voltage (V_H) was estimated after measuring the transverse voltage by sweeping the magnetic field from 9 T to −9 T, and thus subtracting out the resistive contribution. The variation of transverse resistivity (ρ_{xy}) with respect to the applied field measured at 100 K is given in Fig. 8. The transverse resistivity is
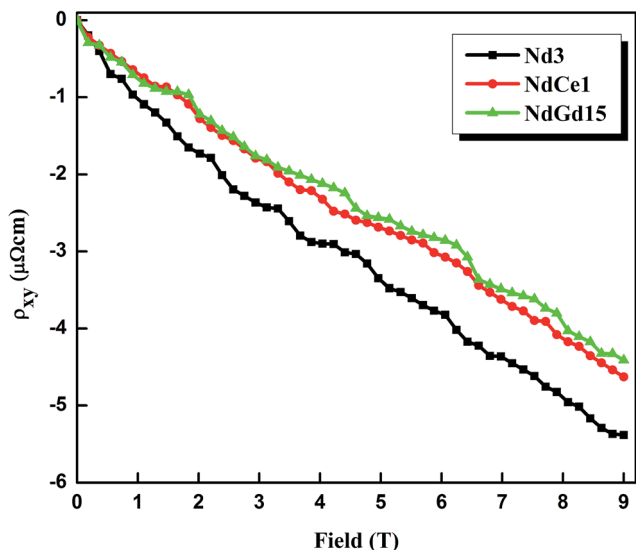
Fig. 8 ρ_{xy} versus T plots of pure (Nd3), Ce doped (NdCe1) and Gd doped (NdGd15) samples measured at 100 K.

found to be negative and exhibits a linear dependence on the applied field for both pure and doped samples. On taking the slope of the linear curves for all the samples, we get the Hall coefficient i.e. $R_H = \rho_{xy}/\mu_0 H$.[30] It is observed that the linear curves for the doped samples NdCe1 and NdGd15 are closer and their respective values of Hall co-efficient are smaller compared to that of Nd3. The R_H values for these samples are -5.6×10^{-9} m³ C⁻¹, -4.8×10^{-9} m³ C⁻¹ and -4.6×10^{-9} m³ C⁻¹ for Nd3, NdCe1 and NdGd15, respectively. The negative R_H values indicate that the majority charge carriers are electrons. On the basis of single band model, the carrier density can be estimated as $n_e = 1/(eR_H)$ and the approximate carrier densities calculated for Nd3, NdCe1 and NdGd15 are 1.1×10^{27} m⁻³, 1.3×10^{27} m⁻³ and 1.35×10^{27} m⁻³, respectively. It is clear that the charge

carrier density of the doped samples is relatively higher than the pure sample, Nd3 at optimum levels of $x = 0.1$ and 0.15 for Ce and Gd doping, respectively.

Fig. 9 shows the magnetic hysteresis loops (MHLs) of pure (Nd3), Ce doped (NdCe1) and Gd doped (NdGd15) Nd1111 samples measured at 5 and 20 K up to a field of 6 T. The hysteresis loop is not symmetric and the width of the loops thin down at high temperature and high field. With the increase in the applied field, the magnetic moment of the samples remains to be negative up to a particular field and thereafter the moment increases, approaches zero and increases further. This point of deviation from linearity gives lower critical field H_{C1} of the samples. Here, the H_{C1} values are 0.12, 0.18, and 0.2 T at 5 K for Nd3, NdGd15 and NdCe1 samples, respectively. It is clearly seen that the hysteresis loop obtained for these samples is a superimposition of a superconducting hysteresis loop on top of a strongly paramagnetic, field-dependent background due to the presence of paramagnetic Nd^{3+} ions present in the sample.[31,32] Taking the mean value of the two branches as the paramagnetic magnetization, $M_P = (M^+ + M^-)/2$, added to the small reversible magnetization of the vortex lattice and subtracting it from the total moment gives the background subtracted magnetization of the samples as shown in insets of Fig. 9a and b. At low fields, the widths are broader and they thin down with field penetration. However, the width of MHLs in the doped samples (NdCe1 and NdGd15) is larger than that in the pure sample (Nd3) at both 5 and 20 K measurements. However, the width of MHLs is larger for NdCe1 as compared to NdGd15. This gives a direct inference that vortex pinning is higher in Ce doped samples.

Further, the superconducting magnetization width (ΔM) due to the critical state of pinned vortices can be estimated as $\Delta M = M^+ - M^-$. Using the extended Bean model and taking the sample dimensions as length scales of magnetization current loops, the global critical current density J_C can be estimated as Global $J_C = 20\left[\Delta M/a\left(1 - \dfrac{a}{3b}\right)\right]$ where ΔM is measured in
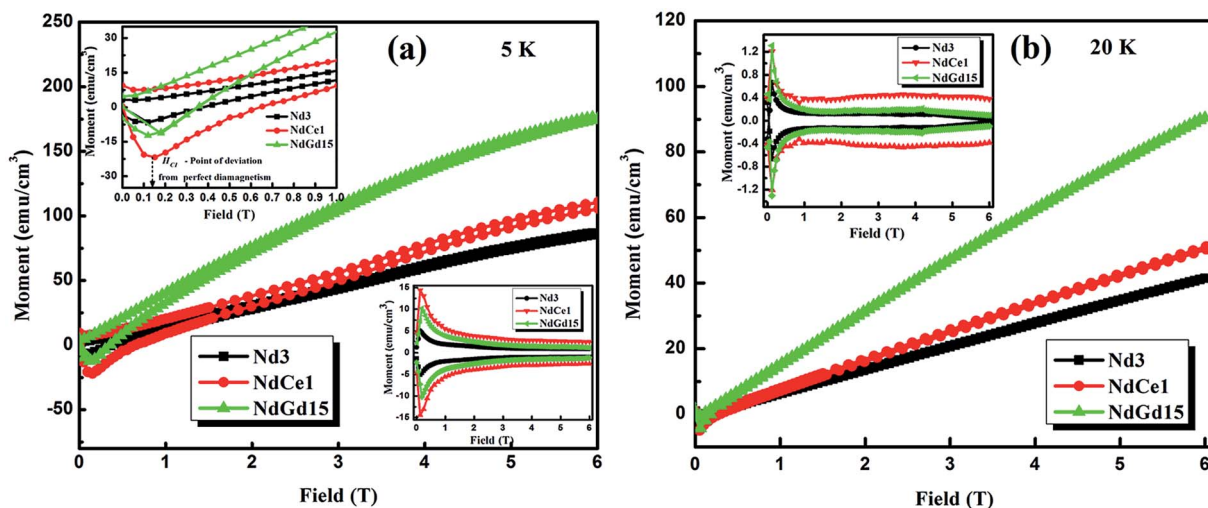

Fig. 9 The magnetic hysteresis loops (MHLs) of pure (Nd3), Ce doped (NdCe1) and Gd doped (NdGd15) Nd1111 measured at (a) 5 and (b) 20 K up to a field of 6 T. Top-left inset of (a) shows the enlarged view around H_{C1}. Bottom-right inset of (a) and inset of (b) show the paramagnetic background subtracted MHLs.
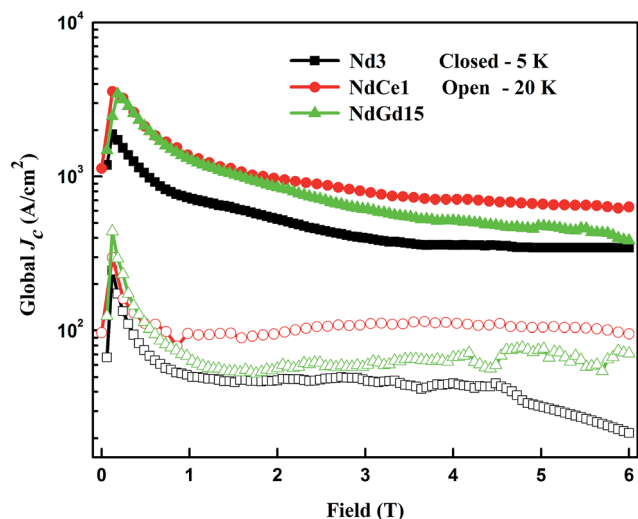
Fig. 10 $J_C(H)$ plots of pure (Nd3), Ce doped (NdCe1) and Gd doped (NdGd15) samples measured at 5 K (closed symbols) and 20 K (open symbols) up to a field of 6 T.

emu cm^{-3}, 'a' and 'b' are the dimensions of the samples with $a < b$ in cm and J_C in A cm^{-2}.[33] The field dependent J_C of pure (Nd3), Ce doped (NdCe1) and Gd doped (NdGd15) Nd1111 samples measured at 5 and 20 K up to a field of 6 T are given in Fig. 10. The J_C of all the samples increases up to H_{C1} and further there is an abrupt decrease in J_C up to an applied field of 1 T. Thereafter, an almost constant J_C is observed for all the samples up to the maximum applied field. The doped samples show competitively better $J_C(H)$ performance in comparison to the pristine sample Nd3. The maximum global J_C observed for Nd3 is 1.8×10^3 A cm^{-2} at 5 K, while for NdCe1 and NdGd15, the J_C is found to be 3.4×10^3 A cm^{-2} at 5 K which is almost double to that of Nd3. Both NdCe1 and NdGd15 trail similar $J_C(H)$ behavior up to 2 T with NdCe1 excelling NdGd15 at higher fields up to 6 T, as expected from the M − H data. At 20 K, the sample Nd3 shows degradation in J_C at higher fields whereas the doped samples still exhibit enhanced J_C with weak field dependence.

The improvement of $J_C(H)$ performance of a superconductor is mainly controlled by the flux pinning centres in it. Often substitution of appropriate dopants creates lattice defects or point pinning centres and sometimes secondary phases or precipitates act as flux pinners.[34] In the present case, both Ce and Gd substitution at Nd site create lattice defects which help in pinning the flux lines on the defects thereby enhancing the current density at applied fields but at higher fields NdCe1 outdo NdGd15. This leads to an inference that lattice defects created due to the substitution of Nd^{3+} with a relatively larger ion Ce^{3+} acts as a stronger flux pinner compared to that due to Gd^{3+}. However, the contribution of secondary phases towards flux pinning is presumed to be minimal since no such secondary phases due to Ce or Gd substitution have been observed within the detection limit of XRD. In the pure sample Nd3 itself, the pinning of flux lines is accomplished by the defects due to fluorine doping at oxygen site. Moreover, $J_C(H)$ measurements and flux pinning studies on single crystals of

different RE1111 systems have already shown that spatial fluctuations of the critical current density do exist on the macroscopic scale and the major contribution comes from collective pinning of vortex lines by microscopic defects by the mean-free-path fluctuation (δK) mechanism.[35] However, substitution of fluorine at oxygen site is also found to create local phase variations, indicating a strong possibility for δT_C pinning mechanism.[36] In the present study, apart from fluorine substitution, the major contribution to vortex pinning is from the substitutional defects due to rare earth doping at Nd site in Nd1111. The presence of mixed phases at low doping levels, observed in the ac susceptibility data of the doped samples, also assists in effective pinning of the flux lines.

To obtain information about the upper critical field (H_{C2}) and flux pinning properties, the temperature dependency of resistivity was measured by applying magnetic fields ranging from 0 to 9 T as shown in Fig. 11. The method of estimating H_{C2} using four-probe resistivity measurement under varying magnetic field provides more accurate values, advantageous over calorimetric measurements which are influenced by the strong paramagnetism of Nd^{3+} ions at high fields.[28,37] Similar to the layered cuprate superconductors, the iron pnictide systems are also reported to have very high critical field and the ρ−T plots under magnetic field variation exhibit a fan-shaped behavior.[38,39] On increasing the field, onset T_C slightly decreased, while the zero resistance temperature or offset T_C largely decreased apparently due to the broadening of the resistivity transition. At the field of 1 T, there is a sudden change in onset T_C. However, the rate of broadening decreases at higher fields. Since the transition temperature does not shift much towards the low temperatures, it indicates to a very high value of $H_{C2}(0)$ (H_{C2} at zero temperature).

The upper critical field H_{C2} and irreversibility field H_{irr} were determined from the 90% and 10% values of the normal state resistivity. In Fig. 12, a graph is plotted with temperatures (T) corresponding to $0.90\rho_n$ (ρ_n – resistivity taken at 56 K) along x-
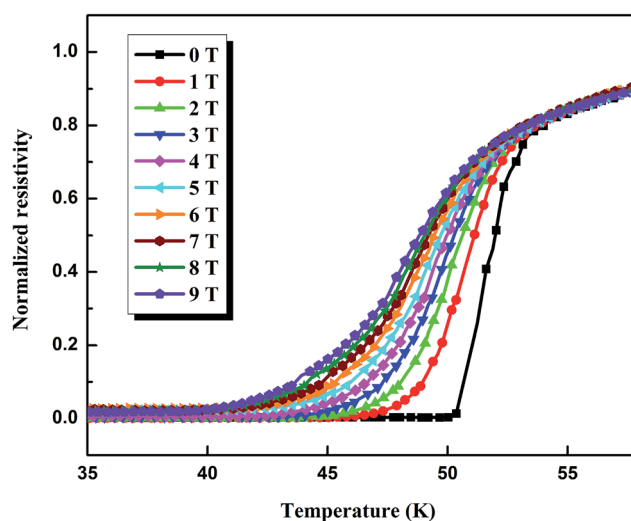

Fig. 11 ρ−T plots of Ce doped (NdCe1) sample measured at fields in the range 0−9 T.
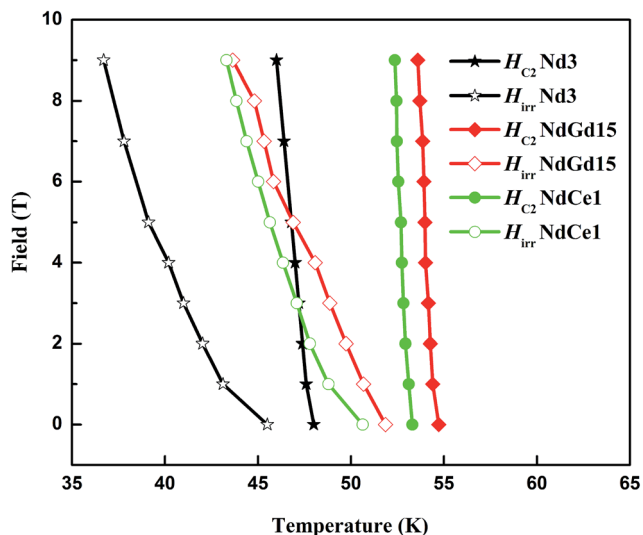
Fig. 12 $H-T$ phase diagram of pure Nd3, Ce (NdCe1) and Gd doped (NdGd15) samples measured at fields in the range 0–9 T.

axis and the respective fields (H) around y-axis. The significant upward curvature of the plots have been already observed in polycrystalline and single crystals of Nd1111 proving it to be an intrinsic feature of oxypnictides rather than a manifestation of the vortex lattice melting or granularity.[37] The slope of this $H-T$ phase diagram *i.e.* $\mathrm{d}(H_{C2})/\mathrm{d}T$ at T_C is used to estimate the H_{C2} on the basis of Werthammer–Helfand–Hohenberg (WHH) theory which is -4.8 T/K, -8.8 T/K and 9.7 T/K for Nd3, NdGd15, and NdCe1, respectively.[40] Accordingly, $H_{C2}(0) = -0.693\ T_C[\mathrm{d}(H_{C2})/\mathrm{d}T]$ has been calculated as 162 T for the pure sample, Nd3; 335 T for the Gd doped sample, NdGd15; and 360 T for the Ce doped sample NdCe1. The estimated values of H_{irr} for Nd3, NdGd15 and NdCe1, are 34.8 T, 42.4 T and 47.5 T, respectively. Earlier studies on single crystal forms of Nd1111 samples have shown a maximum H_{C2} of 304 T using WHH theory.[41] Even though the WHH and Ginzburg–Landau equations seem to be less valid for the low-temperature range, the H_{C2} values estimated using both equations are usually far below the real experimental data; indicating that the real H_{C2} in the samples should be higher than what is estimated from the WHH theory. Thus, it is evident that lattice defects due to rare earth doping, especially Ce doping at Nd site, has been effective in increasing the pinning properties and H_{C2} of pristine Nd1111 thereby making it an ideal candidate for high field applications.

Conclusions

Polycrystalline samples of $NdFeAsO_{0.7}F_{0.3}$ and the doped variants $Nd_{1-x}Ce_xFeAsO_{0.7}F_{0.3}$ and $Nd_{1-x}Gd_xFeAsO_{0.7}F_{0.3}$ were synthesized at ambient pressure to investigate the substitutional effects of relatively larger (Ce^{3+}) and smaller (Gd^{3+}) ions at Nd^{3+} site on the structural and superconducting properties of $NdFeAsO_{0.7}F_{0.3}$. A maximum T_C of 53.6 K and 55.1 K was obtained through Ce and Gd doping at $x = 0.1$ and $x = 0.15$, respectively. At self-field and up to the field of 2 T, both Ce and Gd doped Nd1111 samples exhibit a similar $J_C(H)$ performance

with a magnitude double to that of Nd3. However, at higher fields, the $J_C(H)$ behavior of Ce doped Nd1111 sample is competitive to that of the Gd doped sample. In summary, the smaller ionic size of Gd^{3+} is found to enhance the T_C of Nd1111 while the lattice defects created due to the relatively larger Ce^{3+} ion is found to enhance the $J_C(H)$ performance at high fields.

Acknowledgements

References

1 Y. Kamihara, T. Watanabe, M. Hirano and H. Hosono, *J. Am. Chem. Soc.*, 2008, **130**, 3296–3297.

2 P. M. Aswathy, J. B. Anooja, P. M. Sarun and U. Syamaprasad, *Supercond. Sci. Technol.*, 2010, **23**, 073001.

3 Z. A. Ren and Z. X. Zhao, *Adv. Mater.*, 2009, **21**, 4584–4592.

4 Y. Ma, L. Wang, Y. Qi, Z. Gao, D. Wang and X. Zhang, *IEEE Trans. Appl. Supercond.*, 2011, **21**, 287.

5 Z. A. Ren, W. Lu, J. Yang, W. Yi, X. L. Shen, Z. C. Li, G. C. Che, X. L. Dong, L. L. Sun, F. Zhou and Z. X. Zhao, *Chin. Phys. Lett.*, 2008, **25**, 2215–2216.

6 S. Raghu, X. L. Qi, C. X. Liu, D. J. Scalapino and S. C. Zhang, *Phys. Rev. B: Condens. Matter Mater. Phys.*, 2008, **77**, 220503.

7 C. Wang, Y. K. Li, Z. W. Zhu, S. Jiang, X. Lin, Y. K. Luo, S. Chi, L. J. Li, Z. Ren, M. He, H. Chen, Y. T. Wang, Q. Tao, G. H. Cao and Z. A. Xu, *Phys. Rev. B: Condens. Matter Mater. Phys.*, 2009, **79**, 054521.

8 Y. Li, X. Lin, T. Zhou, J. Shen, Y. Luo, Q. Tao, G. Cao and Z. Xu, *Phys. C*, 2010, **470**, S493.

9 R. H. Liu, G. Wu, T. Wu, D. F. Fang, H. Chen, S. Y. Li, K. Liu, Y. L. Xie, X. F. Wang, R. L. Yang, L. Ding, C. He, D. L. Feng and X. H. Chen, *Phys. Rev. Lett.*, 2008, **101**, 087001.

10 J. L. Yang, W. J. Ren, D. Li, W. J. Hu, B. Li and Z. D. Zhang, *Supercond. Sci. Technol.*, 2010, **23**, 025003.

11 H. Takahashi, K. Igawa, K. Arii, Y. Kamihara, M. Hirano and H. Hosono, *Nature*, 2008, **453**, 376.

12 L. D. Zhao, D. Berardana and N. Dragoea, *J. Alloys Compd.*, 2010, **508**, 606.

13 H. H. Wen, G. Mu, L. Fang, H. Yang and X. Zhu, *Europhys. Lett.*, 2008, **82**, 17009.

14 J. Prakash, S. J. Singh, A. Banerjee, S. Patnaik and A. K. Ganguli, *Appl. Phys. Lett.*, 2009, **95**, 262507.

15 Y. K. Li, X. Lin, T. Zhou, J. Q. Shen, Q. Tao, G. H. Cao and Z. A. Xu, *J. Phys.: Condens. Matter*, 2009, **21**, 355702.

16 Z. A. Ren, J. Yang, W. Lu, W. Yi, X. L. Shen, Z. C. Li, G. C. Che, X. L. Dong, L. L. Sun, F. Zhou and Z. X. Zhao, *Eur. Phys. Lett.*, 2008, **82**, 57002.

17 X. Wang, S. R. Ghorbani, G. Peleckis and S. Dou, *Adv. Mater.*, 2009, **21**, 236.

18 L. Malavasi, G. A. Artioli, C. Ritter, M. C. Mozzati, B. Maroni, B. Pahari and A. Caneschi, *J. Am. Chem. Soc.*, 2009, **132**, 2417.

19 J. B. Anooja, P. M. Aswathy, P. M. Sarun and U. Syamaprasad, *J. Alloys Compd.*, 2012, **514**, 1.

20 S. Vinu, P. M. Sarun, R. Shabna, P. M. Aswathy, J. B. Anooja and U. Syamaprasad, *Phys. B*, 2010, **405**, 4355.

21 G. F. Chen, Z. Li, D. Wu, G. Li, W. Z. Hu, J. Dong, P. Zheng, J. L. Luo and N. L. Wang, *Phys. Rev. Lett.*, 2008, **100**, 247002.

22 Y. J. Cui, Y. L. Chen, C. H. Cheng, Y. Yang, Y. Zhang and Y. Zhao, *J. Supercond. Novel Magn.*, 2010, **23**, 625.

23 C. C. Tang, Y. X. Li, J. Du, G. H. Wu and W. S. Zhan, *J. Phys.: Condens. Matter*, 1999, **11**, 2027.

24 A. Alam and D. D. Johnson, *Phys. Rev. B: Condens. Matter Mater. Phys.*, 2014, **89**, 235126.

25 H. Salamati and P. Kameli, *J. Magn. Magn. Mater.*, 2004, **278**, 237.

26 L. Zhang, X. Leng, S. Y. Ding, X. B. Zhu and Y. P. Sun, *Supercond. Sci. Technol.*, 2010, **23**, 065020.

27 M. Polichetti, M. G. Adesso, D. Zola, J. L. Luo, G. F. Chen, Z. Li, N. L. Wang, C. Noce and S. Pace, *Phys. Rev. B: Condens. Matter Mater. Phys.*, 2008, **78**, 22452.

28 U. Welp, R. Xie, A. E. Koshelev, W. K. Kwok, P. Cheng, L. Fang and H. H. Wen, *Phys. Rev. B: Condens. Matter Mater. Phys.*, 2008, **78**, 140510R.

29 U. Welp, G. Mu, R. Xie, A. E. Koshelev, W. K. Kwok, H. Q. Luo, Z. S. Wang, P. Cheng, L. Fang, C. Ren and H. H. Wen, *Phys. C*, 2009, **469**, 575.

30 P. Cheng, H. Yang, Y. Jia, L. Fang, X. Zhu, G. Mu and H. H. Wen, *Phys. Rev. B: Condens. Matter Mater. Phys.*, 2008, **78**, 134508.

31 C. Tarantini, A. Gurevich, D. C. Larbalestier, Z. A. Ren, X. L. Dong, W. Lu and Z. X. Zhao, *Phys. Rev. B: Condens. Matter Mater. Phys.*, 2008, **78**, 184501.

32 R. Prozorov, E. Tillman, E. D. Mun and P. C. Canfield, *New J. Phys.*, 2009, **11**, 035004.

33 C. P. Bean, *Phys. Rev. Lett.*, 1962, **8**, 250.

34 N. Varghese, K. Vinod, Shipra, A. Sundaresan and U. Syamaprasad, *J. Am. Ceram. Soc.*, 2010, **93**, 732.

35 C. J. Van der Beek, G. Rizza, M. Konczykowski, P. Fertey, I. Monnet, T. Klein, R. Okazaki, M. Ishikado, H. Kito, A. Iyo, H. Eisaki, S. Shamoto, M. E. Tillman, S. L. Bud'ko, P. C. Canfield, T. Shibauchi and Y. Matsuda, *Phys. Rev. B: Condens. Matter Mater. Phys.*, 2010, **81**, 174517.

36 L. Shlyk, K. K. Wolff, M. Bischoff, E. Rose, T. Schleid and R. Niewa, *Supercond. Sci. Technol.*, 2014, **27**, 044011.

37 J. Jaroszynski, F. Hunte, L. Balicas, Y. Jo, I. Raičević, A. Gurevich and D. C. Larbalestier, *Phys. Rev. B: Condens. Matter Mater. Phys.*, 2008, **78**, 174523.

38 F. Hunte, J. Jaroszynski, A. Gurevich, D. C. Larbalestier, R. Jin, A. S. Sefat, M. A. McGuire, B. C. Sales, D. K. Christen and D. Mandrus, *Nature*, 2008, **453**, 903.

39 Y. Jia, P. Cheng, L. Fang, H. Yang, C. Ren, L. Shan, C. Z. Gu and H. H. Wen, *Supercond. Sci. Technol.*, 2008, **21**, 105018.

40 N. R. Werthamer, E. Helfand and P. C. Hohenberg, *Phys. Rev.*, 1966, **147**, 295.

41 Y. Jia, P. Cheng, L. Fang, H. Luo, H. Yang, C. Ren, L. Shan, C. Gu and H. H. Wen, *Appl. Phys. Lett.*, 2008, **93**, 032503.